Influence of kinetics on DDT simulations

O. Dounia [a,*], O. Vermorel [a], A. Misdariis [a], T. Poinsot [b]

[a] Centre Européen de Recherche et de Formation Avancée en Calcul Scientifique (C.E.R.F.A.C.S), France
[b] Institut de Mécanique des Fluides de Toulouse (I.M.F.T), France

Keywords:
DDT
Detailed chemistry
Flame acceleration
Detonation onset
DNS

A B S T R A C T

Deflagration to Detonation Transition (DDT) is an intricate problem that has been tackled numerically, until recently, using single-step chemical schemes. These studies (summarized in Oran and Gamezo, 2007) [1] showed that DDT is triggered when a gradient of reactivity forms inside a pocket of unreacted material. However, recent numerical simulations of hydrogen/air explosions using detailed reaction mechanisms (Liberman et al., 2010; Ivanov et al., 2011) [2,3] showed that detonation waves can emerge from the flame brush, unlike what was usually seen in the single-step simulations. The present work focuses on chemistry modeling and its impact on DDT. Using the idealized Hot Spot (HS) problem with constant temperature gradient, this study shows that, in the case of hydrogen/air mixtures, the multi-step chemical description is far more restrictive than the single-step model when it comes to the necessary conditions for a hot spot to lead to detonation. A gas explosion scenario in a confined and obstructed channel filled with an hydrogen/air mixture is then considered. In accordance with the HS analysis, the Zeldovich's (1970) mechanism [4] is responsible for the detonation initiation in the single-step case, whereas another process, directly involving the deflagration front, initiated DDT in the complex chemistry case. In the latter, a shock focusing event leads to DDT in the flame brush through Pressure Pulse (PP) amplification.

1. Introduction

Mining, process and energy industries suffer from billions of dollars of worldwide losses every year due to gas explo sions. In addition to these costs, explosion accidents are often tragic and lead to severe injuries and fatalities. These damages vary significantly from an a ccident to another, depending on the explosion scenario. A sound knowledge of explosion physics is therefore of vital importance for the prediction of hazard potentials and the implementation of efficient preventive measures.

Gas explosions have been studied experimentally [1,5], theoretically [4,6–11] and numerically [1,12–14]. They occur when a reactive mixture is subjected to an external source of energy from which a combustion wave emerges. This reaction wave can have two possible propagation modes [15,16]: supersonic in the case of detonation and subsonic in the case of deflagration. The direct initiation of detonation has been studied experimentally and theoretically [17–20] and is only possible if a sufficient energy is deposited quasi-instantaneously. In most cases, this condition is not met and a deflagration emerges from the ignition source.

Deflagrations are intrinsically unstable and tend to accelerate continuously after ignition [16]. This Flame Acceleration (FA) process is well understood thanks to extensive experimental (summarized in the Ciccarelli and Dorofeev review paper [5]), theoretical [6–8] and numerical [12,13] works and depends on the degree of confinement and obstruction encountered by the flame during its propagation. FA can either result in fast deflagrations or create the appropriate conditions for the Deflagration-to-Detonation Transition (DDT). Understanding DDT is crucial because it often leads to an escalation in the hazard scenario. Years of theoretical and numerical efforts, have been devoted to exploring the different mechanisms that can initiate DDT. Despite this, a first principle description of the relative importance of these mechanisms, and the possible interplay among them, is still incomplete.

During flame acceleration, the reaction front acts like a piston [15] moving the reactants ahead of it. As a result of the displacement flow, compression waves/shocks are formed ahead of the flame. Thus, a propagating deflagration wave usually consists of the reaction front following a precursor compression wave/shock. This deflagration-shock complex has been tackled by many investigators [9,10,16]. They showed that: (1) the precursor shock is, in general, faster that the deflagration; (2) once the deflagration reaches a critical speed, equal to the sound speed of the burned gases, there exists a path along which a deflagration can reach a veloc-

* Corresponding author.
E-mail address: dounia@cerfacs.fr (O. Dounia).

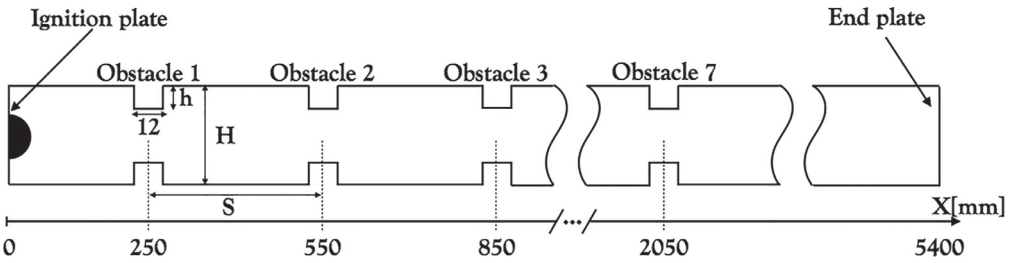

Fig. 1. Sketch of the Gravent explosion channel geometry [26]. A series of 7 obstacles are evenly placed at the top and bottom plates of the channel. The constant spacing S is equal to 300 mm and the blockage ratio is $Br = 2h/H = 30\%$. From the last obstacle to the end plate, the channel is unobstructed allowing detonation propagation without perturbation. Distances are in millimeters.

ity equal to that of the precursor shock, forming a self-sustained detonation wave (or CJ detonation). This path is referred to as the generalized Hugoniot curve by Troshin [11] and basically describes all the successive solutions for the double discontinuity problem during DDT. In other words, according to this simple approach to DDT, a transition to detonation must occur once a certain flame velocity is reached. It does not, however, give a detailed description of the transition itself.

A breakthrough in detonation research occurred when Oppenheim and Urtiew [9,21], later backed up by the simulations of Oran and Gamezo [1], showed that the detonation onset is not simply the result of the coalescence between a flame and a shock. Instead it was observed that the reactants trapped between the leading shock and the deflagration are heated and compressed to the point where enough energy is accumulated and an explosion can occur. These observations are consistent with the mechanism proposed by Zeldovich et al. [4] and later observed experimentally by Lee et al. [22]. Consider a reactive mixture exposed to a gradient of induction time $\nabla\tau_I$, which may be a gradient of temperature or pressure or reactants concentration [23]. A reaction wave emerges from the point of lowest induction time τ_I and its propagation speed depends on $\nabla\tau_I$. For a steep initial gradient, a weak shock forms and quickly detaches from the reaction wave which proceeds as a normal flame. Conversely, for a small initial $\nabla\tau_I$, the mixture is simply uniformly ignited without shock formation. For intermediate values of $\nabla\tau_I$, the reaction wave and the compression waves can propagate in phase. In this case, the coherent energy release causes the compression wave to steepen into a shock. The amplification of the latter and its coupling to a combustion wave later forms a detonation.

The presence of obstacles in the flame path is known [1,24] to facilitate DDT. First, obstructions enhance FA thus producing strong shocks ahead of the flame. Second, these shocks can interact with the obstacles allowing shock focusing at the corners, shock reflections and collisions and shock flame interactions. These events create the appropriate conditions for the detonation onset.

This has been the major trend in DDT research until a recent paper of Kuznetsov et al. [25]. Evaluating the Mach of the shock ahead of the flame prior to DDT, they showed that the temperature of the preheat zone ahead of the flame (550 K for a stoichiometric hydrogen/oxygen mixture) does not allow spontaneous ignition. Therefore, the Zeldovich mechanism could not explain DDT in this case, which raised questions about the universality of the mechanism. Instead Liberman et al. [2] and Ivanov et al. [3] performed numerical simulations with detailed chemistry modeling to show that there exists another mechanism, different from the gradient of reactivity and involving the flame brush, that can explain the transition to detonation.

These last findings suggest that the Zeldovich mechanism is not a universal trigger for DDT, and that the scenario leading to DDT may depend greatly on the chemistry modeling used in numerical simulations. This motivated the present study, which focused on the influence of kinetics on DDT using two-dimensional DNS. The configuration considered is based on the Gravent explosion channel database [26]. The confined and obstructed channel, presented in Section 2, is filled with a quiescent stoichiometric hydrogen/air mixture. The 9S18R (9 species and 18 irreversible reactions) and 3S1R (3 species and 1 reaction) chemical schemes used in this paper are presented in Sections 3.1 and 3.2. These mechanisms are first compared using the canonic Hot Spot (HS) case with constant temperature gradient in Section 3.4. This allows to investigate the requirements, in terms of temperature and radius, for HS to trigger DDT using 3S1R and 9S18R, similarly to the analysis proposed by Liberman et al. [27,28]. The conclusions will be used to explain the results of the simulations of the BR30hS300 channel, presented in Section 4. The impact of the chemistry modeling on the DDT mechanism is analyzed in Section 4.3.

2. Numerical setup

The 2D direct numerical simulations presented in this paper are performed using the DNS/LES solver for the fully compressible multispecies Navier-Stokes equations AVBP, co-developped by CERFACS and IFPEN [29]. A centered continuous Taylor–Galerkin scheme third-order in space and time (TTGC [30]) is used.

To investigate DDT in obstructed and confined channels, the *BR*30*hS*300 configuration of the Gravent database [26] is chosen (Fig. 1). The channel is $H = 60$ mm high and $L = 5400$ mm long. 7 obstacles are evenly spaced along the top and bottom walls of the channel with a constant blockage ratio $Br = 2h/H = 30\%$, where h and H are the height of an obstacle and the channel, respectively. The spacing S between the obstacles axis is equal to 300 mm. From the last obstacle ($X = 2.05$ m) to the closed end wall ($X = 5.4$ m), the section of the channel is constant allowing detonation propagation without perturbation. A three-dimensional DNS of a channel this large is not affordable. Only a two-dimensional longitudinal slice of the *BR*30*hS*300 configuration is therefore considered. Note that 2D simulations of DDT are still largely used nowadays [1] to explore the mechanisms involved in DDT. All obstacles and walls are treated as no-slip adiabatic boundaries.

Usually an Adaptive Mesh Refinement (AMR) is used when simulating DDT in large channels. While this strategy is useful to maintain reasonable computational costs, it requires an a priori knowledge on the key ingredients impacting the problem, thereby increasing the resolution in the regions where these mechanisms activate. Here, another strategy, based on multiple meshes, is used (see Fig. 2). Each grid is stepwise homogeneous and composed of two zones: (1) a refined section, 4.5S large, where the resolution is uniform $\Delta x_{fine} = 20$ μm, thereby allowing to capture the deflagration front (350–450 μm thick), the detonation front (half reaction thickness: 153 μm) as well as the flow structures; (2) a coarser grid, starting at least $2S = 600$ mm ahead of the combustion wave, with a uniform and larger element size $\Delta x_{coarse} = 120$ μm. When the distance separating the tip of the combustion wave from the

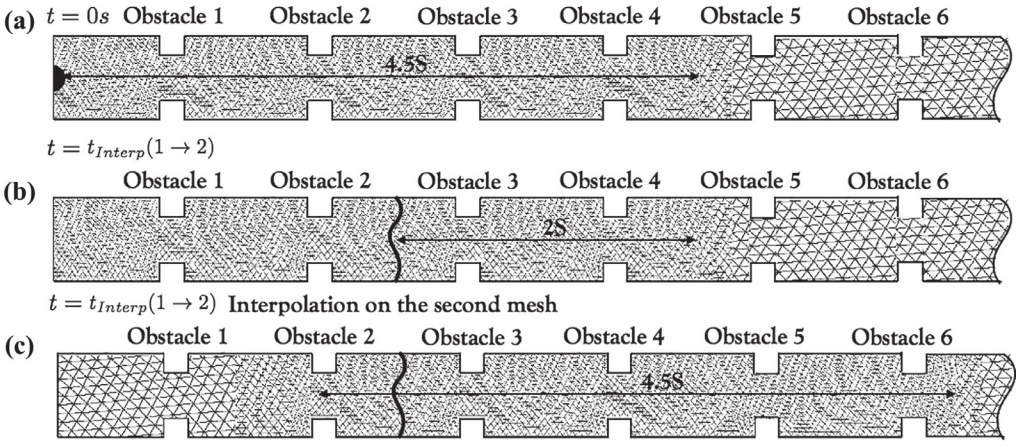

Fig. 2. Illustration of the interpolation procedure between the different meshes used for the present simulations. The interpolation from mesh to mesh is performed when the flame is separated by a distance of two spacings $2S$ from the end of the fine section of the mesh. $t_{Interp}(1 \rightarrow 2)$ denotes the time when the interpolation, from the first mesh to the second, is performed.

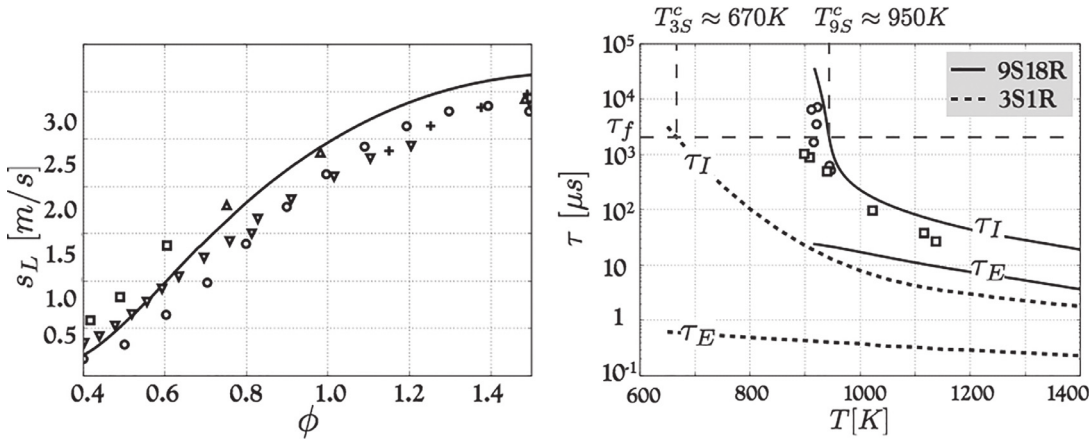

Fig. 3. Left: One dimensional hydrogen/air laminar flame speed s_L at atmospheric conditions for various equivalence ratios ϕ. (Solid line) 9S18R mechanism [31]; experimental data: (□) Berman [38], (○) Dowdy et al. [39], (▽) Egolfopoulos and Law [40], (△) Iijima and Takeno [41], (:) Takahashi et al. [42]. Right: Influence of temperature and chemistry on the induction time τ_I and the excitation time τ_E for $\phi = 1$ and $P = 1$ atm. τ_I from experiments: (□) Slack and Grillo [43] and (○) Snyder et al. [44]. T^c_{9S} and T^c_{3S} are the ignition threshold temperatures for the 9S18R and 3S1R mechanisms, respectively.

end of the refined section reaches $2S$ (Fig. 2(b)), a piecewise linear interpolation of the solution is performed to another mesh with the same characteristics as the previous one except that the refined section now starts just behind the flame tail (Fig. 2(c)). This interpolation is performed 3 times during the flame propagation in the obstructed region without any noticeable numerical noise. It allows to correctly capture the combustion waves as well as the flow structures far ahead of the flame.

The channel is filled with a quiescent mixture of hydrogen and air at atmospheric conditions. It is ignited at the left closed end using a semi-spherical 5 mm radius hot kernel. This initialization procedure was employed in other gas explosion studies ranging from venting deflagrations [12,14] to DDT [1,13]. Among all the equivalence ratios considered in the experiments, the case corresponding to stoichiometric hydrogen/air and showing DDT was selected.

3. Chemistry modeling

The objective of the present paper is to study the influence of the kinetics modeling on DDT. To do so, a single-step reduced chemistry, which is the classical approach for DDT simulations, is confronted to a multi-step mechanism. Besides the chemical scheme, the numerical setup is the same for all simulations.

3.1. Detailed chemistry

The multi-step mechanism chosen to model hydrogen/air chemistry is the mechanism derived by Boivin et al. [31], composed of 9 species and 18 irreversible reactions. This mechanism is referred to as 9S18R in the following. 9S18R is validated against experimental data for atmospheric hydrogen/air laminar flame speeds s_L for a wide range of equivalence ratios $\phi \in [0.4..1.5]$ in Fig. 3(left). The mechanism predicts s_L with very good accuracy at stoichiometry, which corresponds to the case considered for the DDT simulations presented in Section 4.

3.2. One-step reduced chemistry

Until very recently, the most common approach in DDT simulations has been the use of reduced single-step mechanisms [1]. The methodology to derive such chemistries using only one transported species is detailed in [32]. The same procedure was later used by Wang et al. [33] to derive a one-reaction mechanism for hydrogen/air flames, taking into account the reaction order. This strategy was selected to develop the single-step chemistry, named 3S1R, used in the simulations presented in Section 4.

3S1R is designed to reproduce both the flame and the detonation global features. Two fictive species S_1 and S_2 are used, and the reaction formula reads $S_1 + 0.5S_2 \rightarrow \mathcal{P}$, where $\mathcal{P}$ denotes

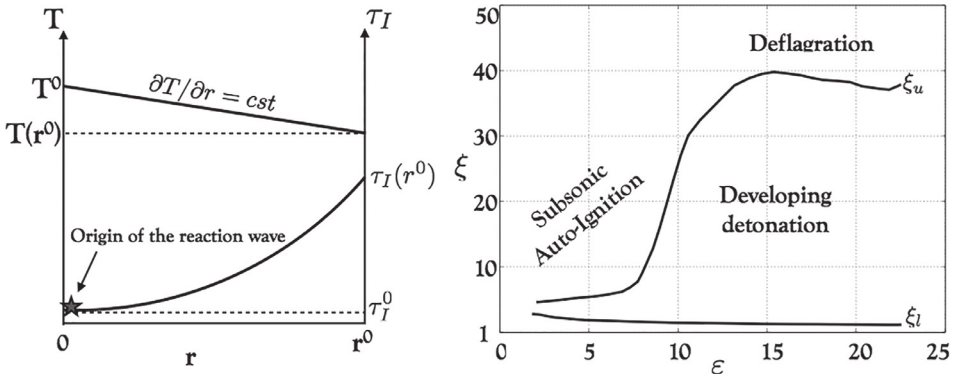

Fig. 4. Left: A sketch of the hot spot (HS) of radius r^0 with constant temperature gradient. The reaction wave emerges from the point of minimum ignition time τ_I. Right: The $\xi - \varepsilon$ diagram shows the detonation peninsula [35]: DDT is possible between the upper branch ξ_u and the lower branch ξ_l.

the products. This allows to mimic the hydrogen oxidation reaction. S_1 and S_2 have the same molecular weight W equal to the average molecular weight of an hydrogen/air mixture at stoichiometry, i.e. $W = 0.021$ kg/mol. Therefore W is constant across the flame. The reactants share the same specific heat capacities at constant pressure C_p and constant volume C_v so that the specific heat ratio γ is constant across the flame front. The Lewis number of the species Le_{S_k} is set to unity. The reaction rate of the irreversible reaction is modeled using an Arrhenius formulation: $\dot{\omega} = A(\rho/W)^{1.5} Y_{S_1} (Y_{S_2})^{0.5} exp(-T_a/T)$. The set of target parameters are:

- The laminar flame speed s_L and the adiabatic flame temperature T_b: they allow the reduced mechanism to reproduce the effect of reactants consumption and gas expansion on the flame propagation during the FA phase. s_L and T_b are imposed equal to the one obtained with the 9S18R mechanism at $\phi = 1$.
- The Chapman–Jouguet detonation speed D_{CJ} and the half detonation thickness δ_d given by the ZND model for the detonation structure. δ_d can be linked to the detonation cell size via empirical relations [1].

To match these targets, a set of parameters can be tuned: the specific heat ratio γ, the chemical energy release Q, the pre-exponential factor A and activation temperature T_a. The values $\gamma = 1.17$ and $Q = 43.28RT_0/\mathrm{M}$ [J/kg] result in the desired targets: $T_b = 7.13T_0$ and $D_{CJ} = 1993$ m/s, $T_0 = 300$ K being the fresh gas temperature and M the mean molar mass of the mixture. Computing the 1D laminar flame in AVBP and the theoretical ZND model using the selected values of γ and Q, the chemical parameters A and T_a are determined so that $s_L = 2.43$ m/s and $\delta_d = 153\,\mu$m. The reaction rate model then reads $\dot{\omega} = 3.9 \times 10^7\ (\rho/W)^{1.5} Y_{S_1} (Y_{S_2})^{0.5} exp(-46.36T_0/T)$ kg/m^3/s.

3.3. Influence of chemistry on ignition characteristic times

DDT involves spontaneous ignition. Therefore, the influence of the chemical scheme on the induction time τ_I and the excitation time τ_E has to be investigated. τ_I is defined as the time for which an homogeneous mixture must be maintained at a given temperature and pressure before exothermic reactions activate. After τ_I, the heat release rapidly blows up and τ_E is defined as the time necessary for the heat release to go from 5 to 100% of its peak value. τ_I and τ_E obtained with 9S18R and 3S1R are displayed in Fig. 3(right) for temperatures in the range [600..1400]K and atmospheric pressure ($\phi = 1$). The τ_I dependance on temperature obtained with the 9S18R mechanism is in good agreement with the experimental data. The ignition threshold T^c is defined here as the temperature below which the induction time needed before ignition is higher than the longest time scale of flame propagation in the BR30S300 configuration $\tau_f = L/s_L \approx 2.2$ ms. This means that when the temperature of the reactants is below T^c, any point on the fresh mixture can be burned by the flame before it can ignite. The ignition threshold $T^c_{9S} \approx 950$ K obtained with the nine-step scheme agrees reasonably well with the experimental data. Conversely, the induction times obtained using the reduced mechanism are orders of magnitude smaller than the experimental data, which coincides with the conclusions of Ivanov et al. [3] regarding τ_I obtained with reduced chemistries for stoichiometric H_2/O_2 mixture. Note that, with 3S1R, the mixture can be ignited even for low temperatures, about 300 K lower than T^c_{9S}. Like τ_I, τ_E obtained with 3S1R are much lower than the ones obtained with 9S18R. The impact of these findings on DDT will be discussed in Section 3.4.

It is important to note that even though detailed mechanisms can reproduce accurately both s_L and τ_I for conditions of pressure lower than 3–5 bar, they suffer from a lack of calibration data for the higher pressure conditions often encountered during DDT. This issue has been mentioned by a number of investigators (see [34]).

3.4. Influence of the chemistry modeling on a canonic DDT problem

In this section, a comparison between the two chemical models is performed with regard to DDT caused by the Zeldovich mechanism [4]. The latter has been designated by a series of DNS [1] as a sufficient condition for DDT onset. The canonic HS problem, sketched in Fig. 4(left) is considered in the following.

3.4.1. The hot spot problem and the detonation peninsula

According to Zeldovich and co-workers, a detonation can emerge from a hot spot, i.e. a region characterized by a gradient of induction time $\nabla\tau_I$ [4]. Inside the hot spot, a combustion wave forms at the point of minimum τ_I. If $\nabla\tau_I$ is too steep, a shock forms and separates from the combustion wave. The latter proceeds as a deflagration. On the other hand, if $\nabla\tau_I$ is too small, the entire hot spot is ignited uniformly. For an intermediate range of $\nabla\tau_I$ however, a coupling between the shock and the combustion wave is possible. A positive feedback between the two waves eventually leads to the formation of a detonation front.

Bradley and Kalghatgi [35] characterized the gradient of induction time $\nabla\tau_I$ needed to trigger DDT. Inside the hot spot, both a reaction wave and a compression wave are formed. To allow a resonance between both waves, the reaction wave velocity $u_I = dx/d\tau_I$ must neither be too high nor too low compared to the compression wave velocity (sound speed) a. A comparison between u_I and a can be made through the variable $\xi = a/u_I$. For certain values of ξ allowing resonance, the compression wave can gain in amplitude if the heat release inside the reaction wave is deposited

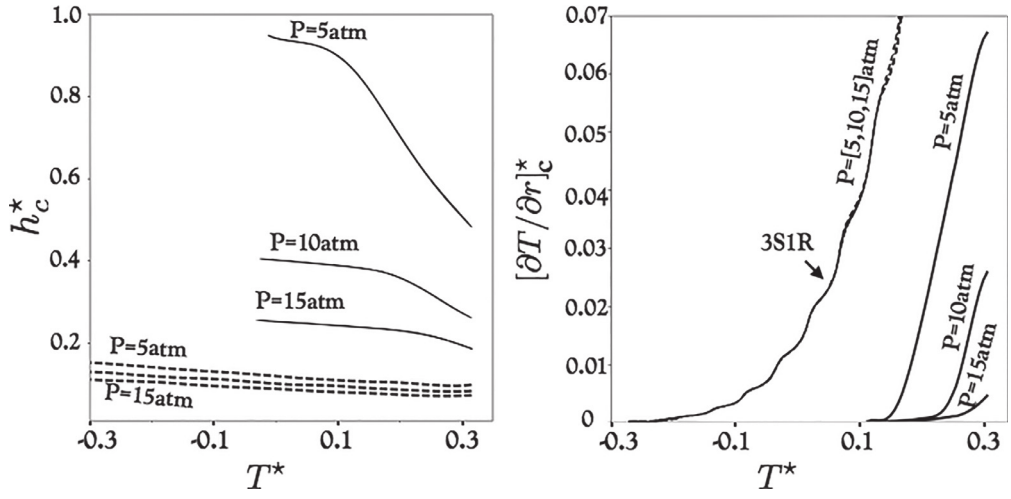

Fig. 5. The influence of pressure P and temperature $T^\star$ on critical HS parameters for the single-step (dashed lines) and the multi-step mechanisms (solid lines). Left: $h_c^\star$ is the minimum non-dimensional size that allows energy input to pressure waves, i.e. $\varepsilon_c = 1$. Right: $[\partial T/\partial r]_c^\star$ is the minimum non-dimensional temperature gradient that allows resonance between pressure and reaction waves, i.e. $\xi_c = 1$.

fast enough. This can be characterized by introducing the variable $\varepsilon = r^0/(a\tau_E)$, where ε measures the chemical energy fed to the pressure pulse during its residence inside a hot spot of radius r^0. A region in the $\xi - \varepsilon$ space, called the detonation peninsula [35], has been identified as the region where the conditions at the hot spot are ideal for the onset of detonation. The region is illustrated in Fig. 4(right), between the upper branch ξ_u and the lower branch ξ_l.

3.4.2. The influence of chemistry modeling on the hot spot scenario

In this section, the $\xi - \varepsilon$ diagram is used to investigate the outcome of a hot spot using the 9S18R and the 3S1R mechanisms. Consider a hot spherical kernel with a constant temperature gradient and a non-dimensional size $h^\star = 2r^0/h$, where h is the height of an obstacle in the BR30hS300 channel (see Fig. 4). The non-dimensional peak temperature inside HS is defined as $T^\star = (T^0 - T^c)/T^c$, where T^c is the ignition threshold. Negative values of $T^\star$ indicate temperatures at which the mixture will not be ignited. Since the values T^c obtained with 9S18R agree very well with the experimental data, at least for atmospheric conditions, T^c is set equal to T^c_{9S}.

The $\xi - \varepsilon$ plane offers two limit lines: (1) the minimum energy input $\varepsilon_c = 1$, (2) the perfect resonance between compression and combustion waves $\xi_c = 1$. These limits allow to define critical hot spot parameters that can trigger DDT: (1) $h_c^\star$ is the minimum non-dimensional HS size where pressure waves can travel to gain energy, i.e. $h_c^\star = 2\varepsilon_c(a\tau_E)/h$; (2) ξ can be reformulated [35] as $\xi = a(\partial T/\partial r)(\partial \tau_l/\partial T)$ in the radial coordinates, thereby the minimum HS temperature gradient that leads to a resonance between pressure and reaction waves can be expressed as $[\partial T/\partial r]_c = \xi_c/(a\partial\tau_l/\partial T)$. A non dimensional form for $[\partial T/\partial r]_c$ is then $[\partial T/\partial r]_c^\star = (T^0/h_c)[\partial T/\partial r]_c$, where $h_c = h_c^\star h$. $h_c^\star$ and $[\partial T/\partial r]_c^\star$ depend on the conditions of pressure P and temperature $T^\star$ inside the hot spot. The influence of P and $T^\star$ as well as the chemical scheme on the critical HS parameters is assessed in Fig. 5. Because τ_E is much higher for the multi-step chemistry, $h_c^\star$ values obtained with 9S18R are higher than those obtained with 3S1R, independently of the temperature. For relatively low pressure ($p = 5$ atm), the critical hot spot size is higher than half an obstacle height (h) and tends to h as the temperature becomes close to the temperature threshold. Increasing the pressure leads to a radical decrease of $h_c^\star$ to meet values close to the one obtained with the single-step mechanism. This implies that, for this canonic scenario and when using detailed hydrogen/air schemes, conditions where energy can be fed to pressure waves can only be obtained when strong shocks are involved, resulting in drastic pressure increase. This conclusion was also reached by Ivanov et al. [3] and Liberman et al. [27,28] who computed the hot spot problem with a more detailed hydrogen/air reaction scheme. Note that, for the single-step mechanism, conditions where HS can lead to an increase in pressure waves amplitude can be met even for temperatures lower than the ignition threshold ($T^\star < 0$). Figure 5(Right) shows that for the 3S1R case, there exists a temperature gradient for which DDT can occur for a large temperature range, and for conditions below the ignition threshold. Increasing the hot spot peak temperature results in an increase in the minimum temperature gradient. On the other hand, the multi-step scheme allows DDT for high temperatures only ($\geq$ 1100 K). As the pressure increases, the DDT region tends towards higher temperatures also pointing out the need for strong shocks. Note that the single-step mechanism shows almost no pressure dependance.

The hot spot problem may represent a simplified scenario far from the realistic conditions that lead to DDT in gas explosions. In practice, the hot kernel is certainly non-spherical and the distribution of the temperature gradient can be heterogeneous. In addition, reactants mixing can occur leading to additional reactivity gradients. However, Fig. 5 suggests that the single-step approach allows DDT to occur for conditions far less restrictive than those required by the detailed hydrogen/air chemistry. The latter, which is validated against experimental data, may not even allow DDT via gradient of reactivity in configurations such as the *BR30hS300* channel, unless strong shocks are formed. Further investigation is needed to assess the extent of such conclusions to other mixtures and fuels.

4. Numerical simulation of the BR30hS300 configuration

4.1. Flame speed and DDT

The conclusions of the previous section are assessed on a more complex scenario of DDT in a confined and obstructed channel. The explosion scenario of the BR30hS300 [26] is computed using the single-step and multi-step mechanisms. The evolution of the non-dimensional flame tip velocity s_{tip}/D_{CJ} versus the flame tip position is displayed in Fig. 6(left). The flame tip position is defined by $c = Y_{H_2}/Y_{H2,u} = 0.95$ for the detailed chemistry and $c = Y_{S_1}/Y_{S_1,u} = 0.95$

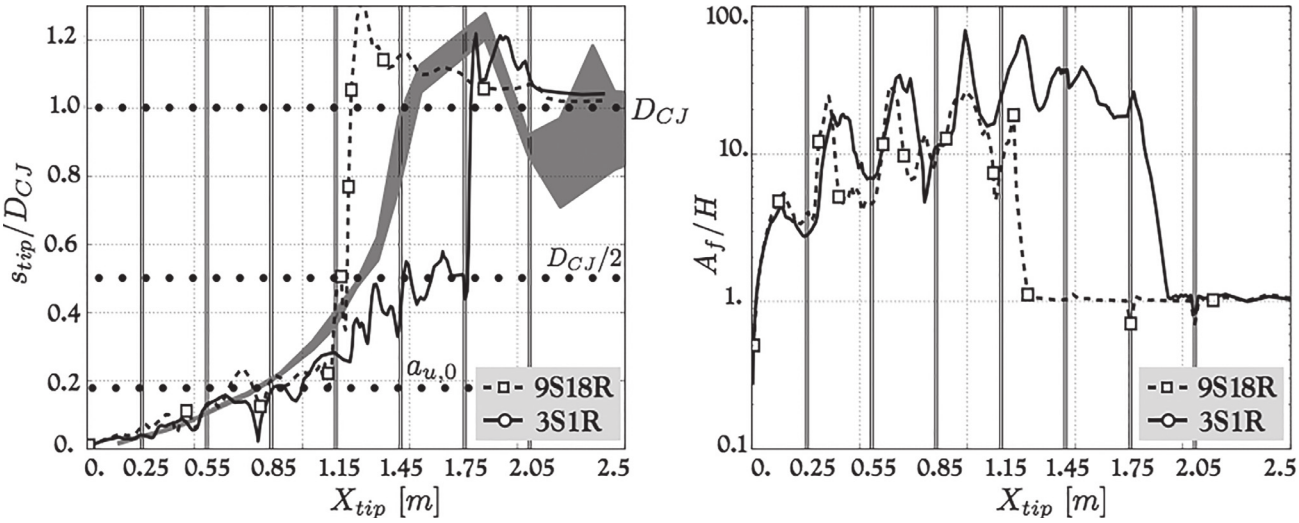

Fig. 6. Evolution of the non-dimensional flame tip speed (left) and non-dimensional flame surface (right) with the flame tip position. The gray area represents the experimental shots. The vertical bars represent the position of the seven obstacles. $a_{u,0}$ is the sound speed at the fresh gases for the initial conditions.

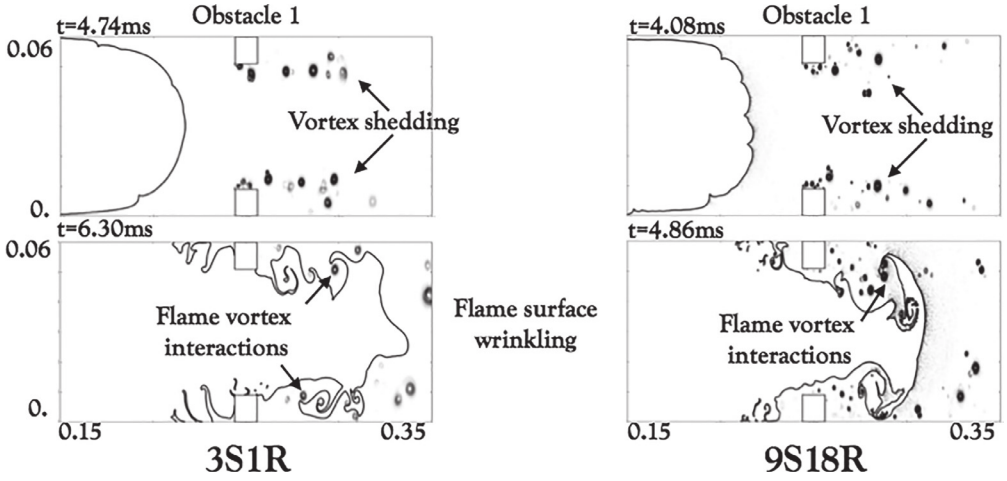

Fig. 7. Numerical Schlieren ($\nabla\rho/\rho$) and isocontour of progress variable $c = 0.5$ showing the flame interaction with the first obstacle. Left: single-step mechanism. Right: Multi-step mechanism.

for the single-step mechanism, where u denotes unburned gases. The numerical simulations correctly capture the main features of the experiment. Upon ignition, the flame undergoes multiple accelerations, which are well reproduced by both chemical mechanisms. This can be explained by the fact that 3S1R and 9S18R share the same laminar flame speed s_L and burnt gas temperature T_b, which allows a good prediction of reactants consumption and gas expansion during flame propagation. In addition, according to Joulin and Mitani [36] and Sun et al. [37], the effective Lewis number Le_{eff} of two reactants flames depends on the reaction order, the equivalence ratio and the Lewis number of the reactants. Le_{eff} reduces to the lewis number of the fuel (oxydizer) in the case of very lean (rich) flames. In between, a gradual evolution of Le_{eff} is observed. At stoichiometry, Le_{eff} is close to unity for hydrogen/air flames, which: (1) depletes thermo-diffusive instabilities (confirmed by the experiment); (2) makes the flame speed response to stretch identical for both chemistries.

Before the first obstacle, FA is laminar in nature and is induced by the strong channel confinement (high S/H ratio). The latter quickly forces the flame to transition from the spherical to the finger shape with a rapid increase in flame surface as seen in Fig. 6(right). The obstacles ahead of the flame enhance FA with successive and stronger flame surface increases, until a sharp increase in flame speed is observed, indicative of a transition from deflagration to detonation.

While both mechanisms predict DDT, its location is strongly impacted by kinetics. Nevertheless, DDT was observed in both simulations just one section either before (9S18R) or after (3S1R) the one predicted by the experiments. Prior to DDT, both flames have reached the fast propagation regime: s_{tip} is equal to $0.4D_{CJ}(0.5D_{CJ})$ for the 9S18R (3S1R respectively) case. The value $D_{CJ}/2$ is equal to the CJ deflagration speed and corresponds to the maximum deflagration speed [16]. Figure 6 shows that, in the 3S1R case, the flame acceleration process slows down when this limit value is reached ($X \in [1.45, 1.75]$m). The flame surface also reaches a plateau at this regime. After the abrupt DDT process, and in accordance with experimental data, the flame propagation speed reaches a quasi-steady value close to the predicted autonomous detonation speed D_{CJ}. The non-dimensional flame surface A_f/H then quickly relaxes to unity showing that a quasi-planar detonation propagates in the channel.

The flame acceleration phase, as a necessary step for creating the appropriate conditions for DDT, is briefly analyzed in Section 4.2. Then, the flow conditions prior to DDT are investigated in details in Section 4.3 to determine whether the ingredients that lead to detonation are identical for both chemistries.

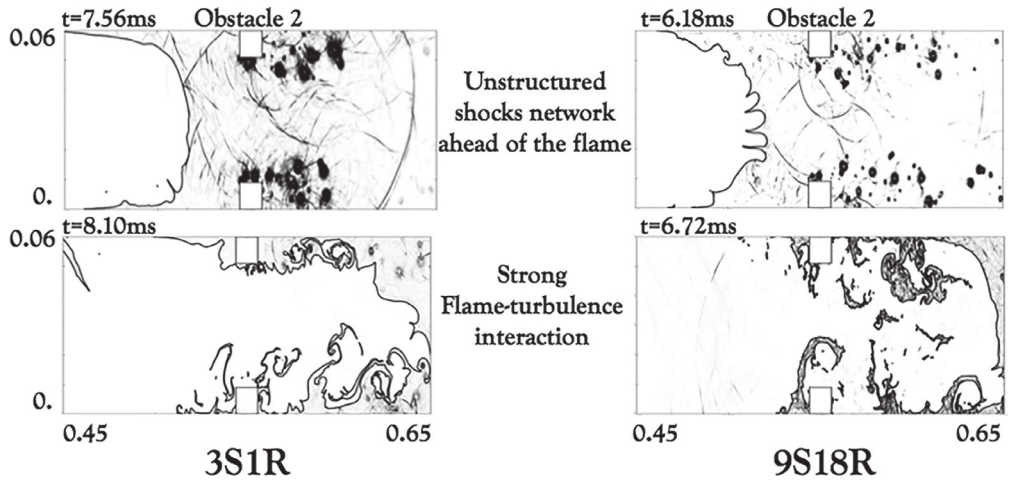

Fig. 8. Numerical Schlieren ($\nabla\rho/\rho$) and isocontour of progress variable $c = 0.5$ showing the shocks network formed ahead of the flame. Left: single-step mechanism. Right: Multi-step mechanism.

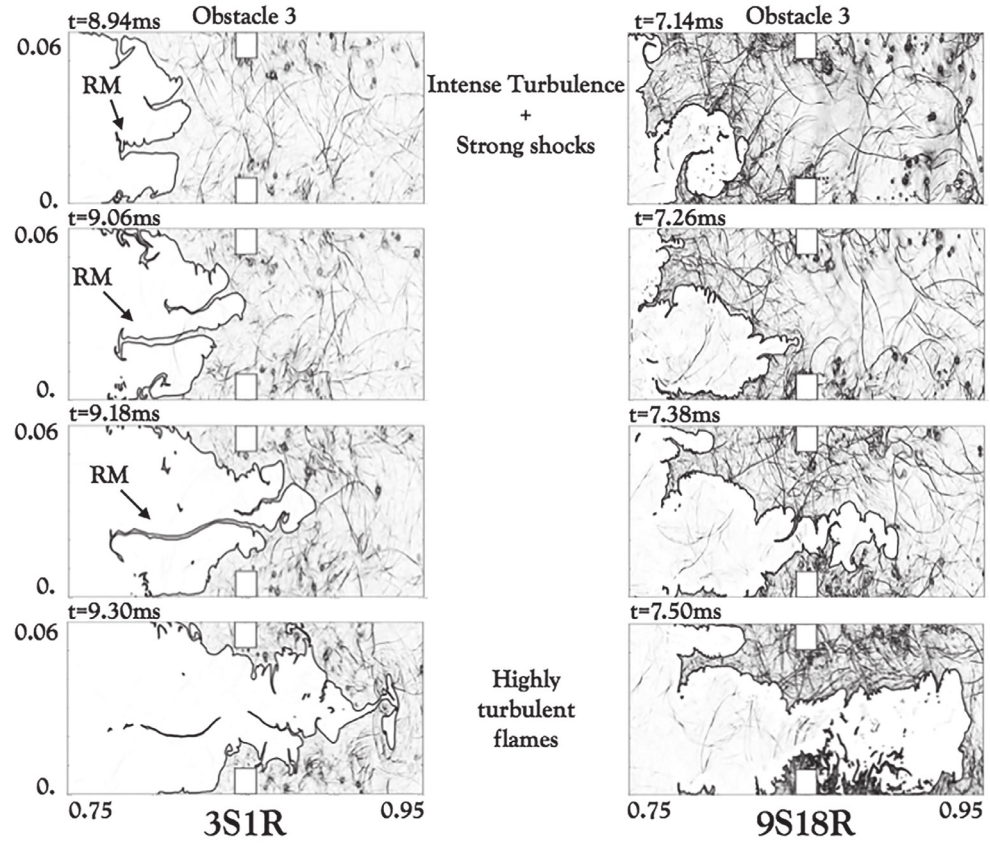

Fig. 9. Numerical Schlieren ($\nabla\rho/\rho$) and isocontour of progress variable $c = 0.5$ showing the highly turbulent flame crossing the third obstacle. RM denotes the Richtmyer–Meshkov (RM) instability. Left: single-step case. Right: multi-step case.

4.2. FA phase

Few microseconds after ignition, the flame undergoes the first acceleration episodes due essentially to confinement (finger flame [7]). Starting from the first obstacle, additional FA mechanisms are triggered. The first one is related to the sudden flow contraction. The fresh gases, pushed by the reactive piston, are accelerated when they penetrate the congestion. When the flame starts interacting with the obstacle, the jump velocity condition induces a sudden increase of the flame speed. This mechanism is however limited to the vicinity of the obstacle. The FA process continues downstream of the first congestion because of the flame interaction with the flow structures. When the tip of the combustion wave exits the congestion, the remaining part of the reactive surface journeys in a turbulent flow (where vortex shedding has been triggered earlier). Consequently, the flame front is wrinkled as illustrated in Fig. 7 for both chemistries. Flame vortex interactions account for the strong increase of the flame surface just downstream of the congestion observed in Fig. 6(right). Because of the large obstacle spacing to channel height ratio ($S/H = 5$), the contribution of the congestion to the flame acceleration stops a certain distance away from the obstacle and the flame surface

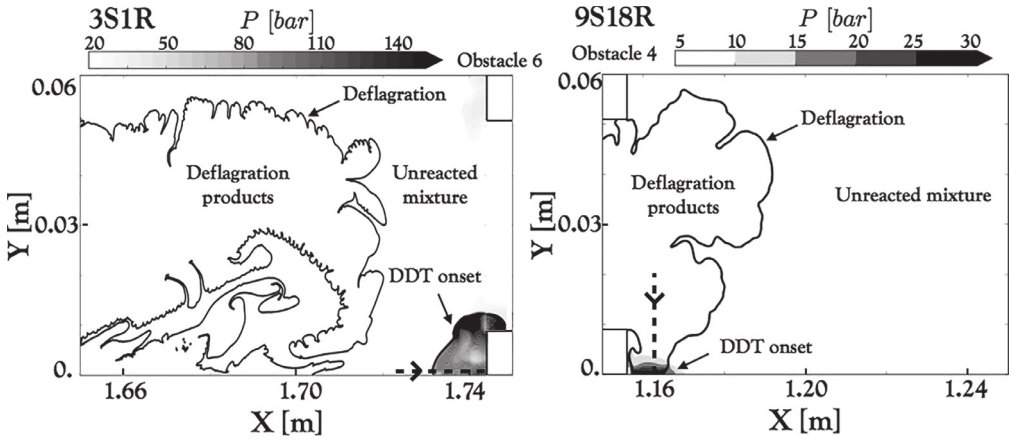

Fig. 10. Zoom on the onset of detonation. Pressure field and isocontour of progress variable $c = 0.5$ are displayed. The dashed lines correspond to a cut through which DDT is analyzed in Sections 4.3.1 and 4.3.2. Left: single-step case. Right: multi-step case.

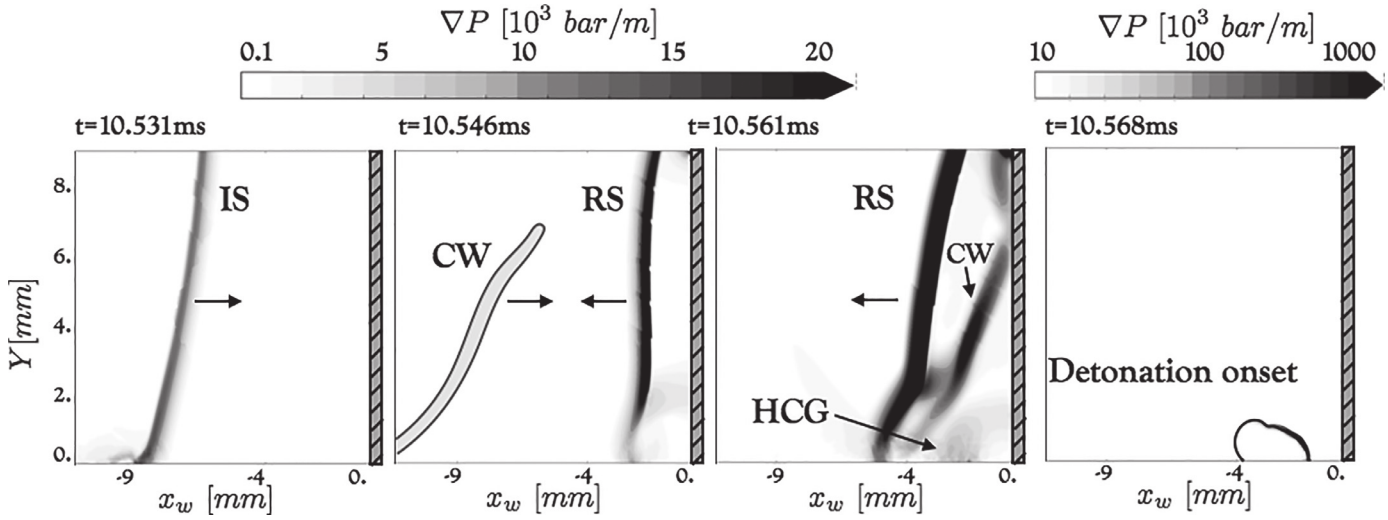

Fig. 11. Key events surrounding the detonation onset for the 3S1R simulation. Pressure gradient ∇P is displayed. x_w represents the distance from the obstacle 6 left wall (grey dashed area). IS is the incident shock. RS and CW indicate the reflected shock and a compression wave, respectively. HCG stands for Highly Compressed Gas. A detonation wave is triggered at $t = 10.561$ ms and propagates along the obstacle.

drops significantly. This explains the repeated flame acceleration–deceleration phases observed for both chemical mechanisms in Fig. 6.

Contrary to the deflagration-precursor shock structure observed in smooth channels [9,21,25], repeated shock reflections at the obstacles result in an unstructured shock network ahead of the flame (Figs. 8 and 9). When leaving the second obstacle, the flame is highly turbulent as seen at $t = 8.10$ ms ($t = 6.72$ ms) for the single-step (multi-step) mechanism, respectively.

Shock reflections at the obstacles allow flame-shock interactions. This is highlighted in Fig. 9 in the 3S1R case where a Richtmyer–Meshkov (RM) instability is triggered with a large funnel of unburned material penetrating the region of burnt gases. This instability further contributes to the increase of the flame surface. Until the fourth obstacle, FA in both simulations matches reasonably well. The reason why DDT is observed first with the detailed chemistry and delayed with the reduced mechanism is discussed in the next section.

4.3. Detailed analysis of DDT onset

The detonation onset location is strongly impacted by the chemistry modeling as shown in Fig. 6. There may be two possible explanations for this: (1) the DDT mechanism is the same but the necessary conditions to trigger it are met earlier in the 9S18R case than the 3S1R case; (2) the mechanism is different and involves different ingredients to initiate detonation. A first step towards identifying the key elements responsible for DDT in both simulations is to look at the DDT location. Figure 10 displays the pressure field when the detonation wave starts to form. In both cases, DDT occurs close to the obstacles, in regions of highly compressed gas. In the 3S1R case, DDT starts in the unreacted mixture ahead of the deflagration front. On the other hand, DDT seems to take place either in the flame brush or between the flame and the wall for the 9S18R case. Figure 10 suggests that the deflagration may play a role in the DDT scenario with 9S18R.

Given the seemingly particular nature of the DDT scenario in the 9S18R case, a grid independence study has been carried out to ensure that this mechanism is not induced by numerical artefacts. Therefore, the computation was also performed with another mesh where the grid resolution has been increased around the DDT location shown in Fig. 10(Right). This refined mesh is composed of a window 300 mm large and centered around the DDT location. The mesh size in this window is 10 μm, which is about half the size of the smallest cells in the reference mesh. Details on this grid independence study are given in the annexe section. It shows that an identical scenario takes place with the refined mesh, thereby confirming the mechanism. In the following, the detailed analysis

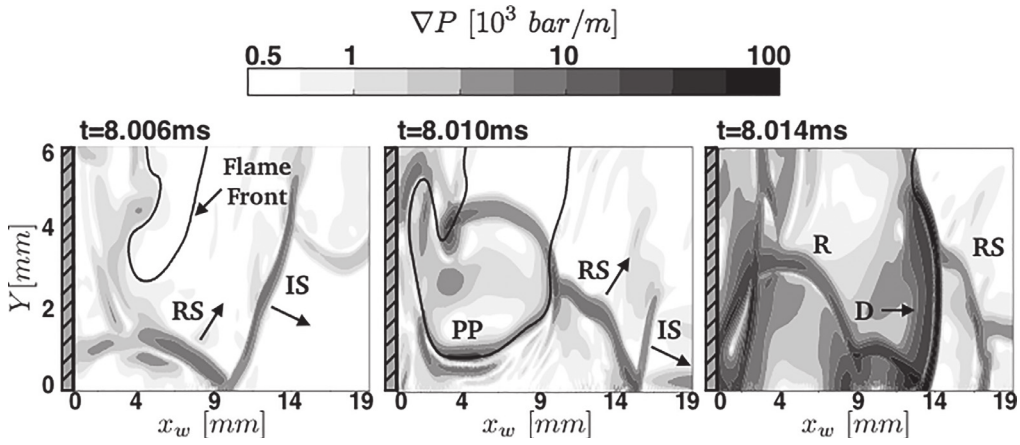

Fig. 12. Key events surrounding the detonation onset for the 9S18R simulation. Pressure gradient ∇P is displayed. x_w represents the distance from the obstacle 4 right wall (gray dashed area). The flame front is represented by the isocontrour of progress variable $c = 0.5$. *IS* and *RS* denote the incident shock and the reflected shock, respectively. *PP* is the pressure pulse observed prior to the detonation onset. *D* and *R* represent the detonation wave and the retonation wave, respectively.

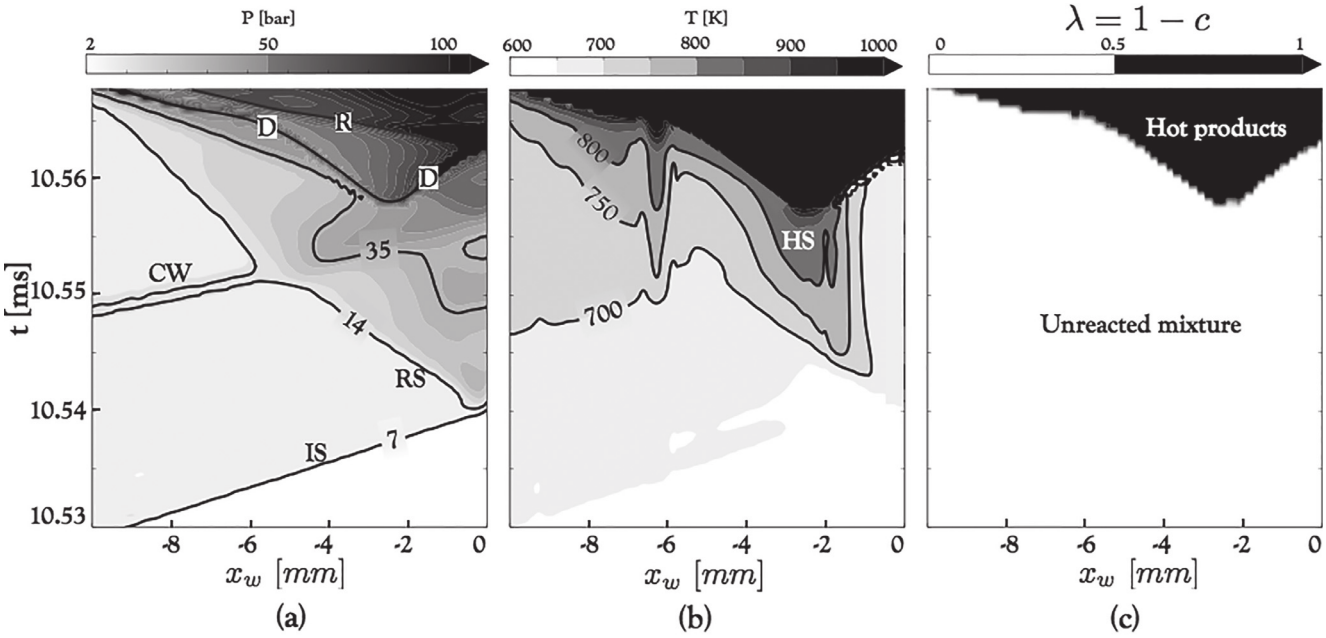

Fig. 13. Time evolution of pressure (a), temperature (b) and $\lambda = 1 - c$ (c) in the single-step case through the cut line presented in Fig. 10(Right), positioned 500μm from the bottom wall. x_w is the distance from the obstacle 6 left wall. IS, RS, CS, R and D denote an incident shock, a reflected shock, a compression wave, the retonation wave and the detonation wave, respectively. HS is a hot spot.

of the DDT event in the 9S18R case is conducted on the refined mesh, since it enables a finer description of the phenomenon.

Figures 11and 12 focus on the moments surrounding DDT for the single-step and the multi-step mechanisms, respectively. For the 3S1R case, an Incident Shock (IS) gets reflected at the sixth obstacle ($X = 1.744$ m) and a Compression Wave (CW) is seen coming in the opposite direction to the reflected shock (RS). The collision between CW and RS leads to the formation of a highly compressed and heated region (HCG) from which a detonation wave emerges a few microseconds later. A detailed analysis of the detonation onset in this case is performed in Section 4.3.1. Shock reflection is also involved in the DDT process in the detailed chemistry case but the scenario is completely different. Figure 12 shows that, as a consequence of the reflected shock crossing the flame path, a Pressure Pulse (PP) forms at the flame front and leads to detonation initiation inside the flame brush. This confirms that the deflagration is indeed an active participant in the DDT mechanism observed for the 9S18R case. DDT in the flame brush triggered by the head-on collision of a shock with a flame front was also observed recently by Goodwin et al. [24]. This scenario is analyzed in Section 4.3.2.

4.3.1. Single-step chemistry and the Zeldovich mechanism

DDT in the 3S1R case takes place in the unreacted mixture as already observed in other simulations [1]. The detonation wave is initiated behind the reflected shock observed in Fig. 11. To understand the effect of this shock on the gas and its role in the DDT process, the simulation is inspected through the cut line presented in Fig. 10(Right), positioned 500 μm from the bottom wall. The result is displayed in Fig. 13.

The propagation of *IS, RS* and *CW*, shown in Fig. 11, can be observed in Fig. 13(a,b). As a result of the incident shock reflection on the obstacle, a pressure and temperature increase can be observed behind RS. The latter can interact back with the boundary layer and a further increase of temperature is observed due to viscous heating. A region of hot unburned gas ($T \geq 750$ K) can then be observed at the RS tail. The collision of the reflected shock with

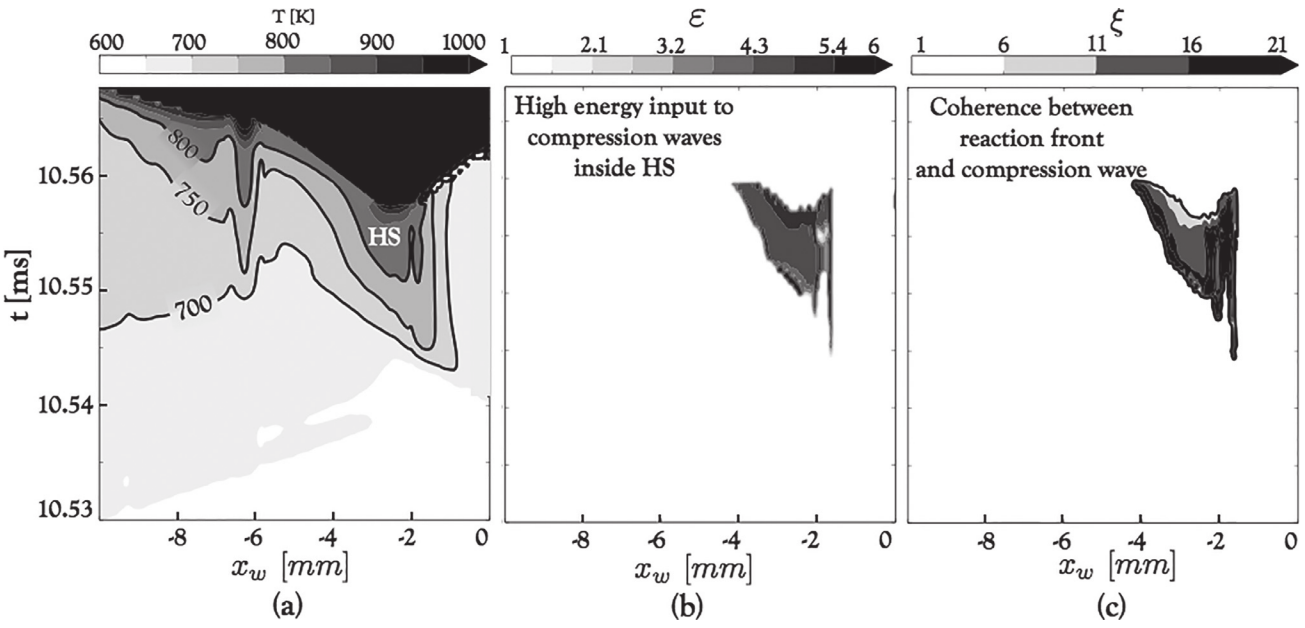

Fig. 14. Time evolution of temperature (a), ε (b) and ξ (c) in the single-step case through the cut line presented in Fig. 10(Right), positioned 500 µm from the bottom wall. x_w is the distance from the obstacle 6 left wall. IS, RS, CS, R and D denote an incident shock, a reflected shock, a compression wave, the retonation wave and the detonation wave, respectively. HS is a hot spot.

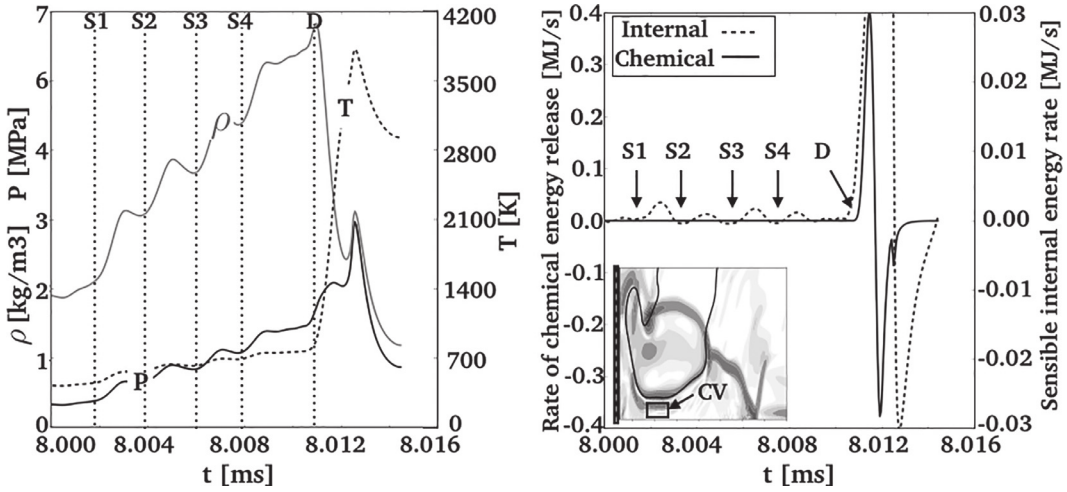

Fig. 15. Temporal evolution of key parameters integrated along the control volume (CV) shown on the right figure: (Left) Temperature, pressure and density; (Right) Chemical energy release rate and sensible energy release rate. *S*1 – 4 mark a series of four consecutive shock compressions. *D* marks the moment the mixture detonates.

a compression wave propagating in the opposite direction leads to the formation of a region of hot ($T \geq 800$ K) and highly compressed ($P \geq 35$ bar) unburned reactants called Hot Spot (*HS*). A detonation wave clearly emerges from *HS* as a strong shock (see Fig. 13(a)) propagates away from HS, coupled to a reaction wave suggested by the formation of combustion products behind it in Fig. 13(c). A retonation wave can be observed in Fig. 13(a) as a result of the reflection of the detonation front on the obstacle. The conditions in pressure and temperature observed inside HS are caused by the strong leading shock (IS) reflecting off the wall. This explains why DDT was delayed until the sixth obstacle in this case, allowing the leading shock to gain in strength while the flame propagates in the channel.

To understand why a detonation wave emerges from the hot spot, the evolution of the variables ε and ξ is displayed in Fig. 14. The formation of the hot unburned region HS coincides with values of ε higher that unity. This means that in HS, a compression wave can form and gain in amplitude as its residence time in HS is higher than the time needed locally for the mixture to deliver chemical energy. On the other hand, in the hot spot, for $T \leq 800$ K, high values of ξ are met, since the gradient $\partial\tau_I/\partial T$ is high for low values of temperature. The increase in temperature inside HS leads to higher values of energy input to pressure waves $\varepsilon \geq 5$ just prior to DDT and lower values of ξ. This means that the evolution of HS was towards high energy transmission to pressure waves ($\varepsilon\nearrow$) and resonance between the latter and the reaction fronts that emerge from HS ($\xi \to 1^+$). The initiation of the detonation wave in the case 3S1R is therefore the result of the classical Zeldovich mechanism.

Note that the temperature conditions met inside the hot spot are not high enough to initiate a detonation via the Zeldovich mechanism if the multi-step mechanism was used instead. Indeed, the flame residence time inside an obstructed section can be defined as $\tau_f = S/(D_{CJ}/2) \approx 300\,\mu s$. Therefore, to allow ignition at these conditions in pressure (i.e. $\tau_I \leq \tau_f$), the minimum temperature inside the hot spot should be higher that 1100 K, which would

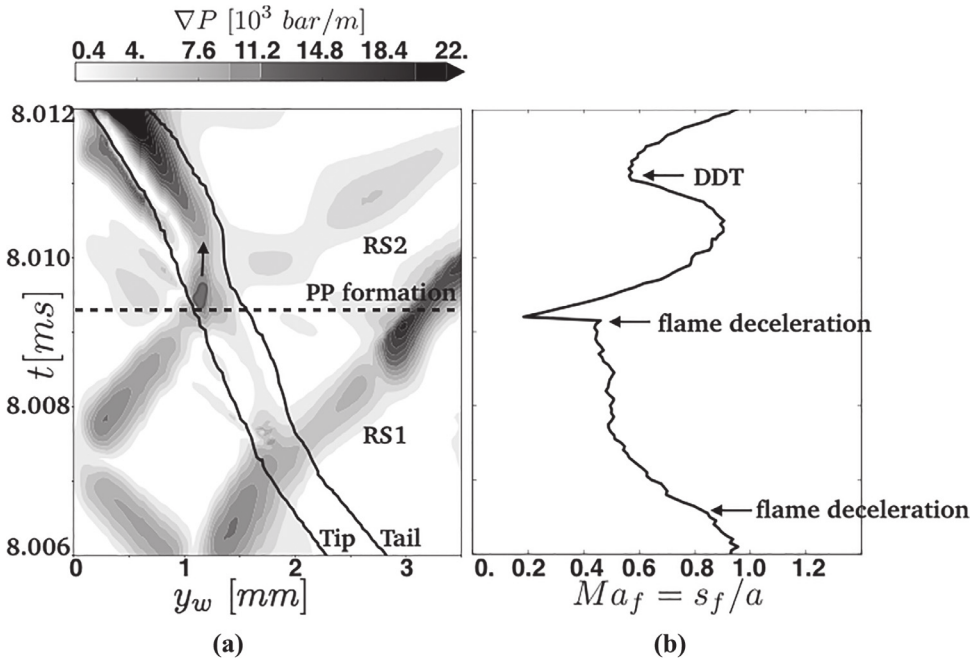

Fig. 16. (a) Temporal evolution of the pressure gradient for the multi-step case through the cut line presented in Fig. 10(Left). y_w is the distance to the bottom wall. *RS*1 and *RS*2 are two reflected shocks. *D* denote the detonation wave. The black contours indicate the flame tip and tail. (b) Local flame Mach number Ma_f. s_f is the propagation speed of the closest point on the flame front to the bottom wall.

have required a much stronger shock IS than the one observed in the 3S1R simulation.

4.3.2. Detailed chemistry and pressure pulse amplification

Similarly to what was done by Goodwin et. al. [24], who observed seemingly the same mechanism as the one shown here for the 9S18R case, a control volume analysis is performed on a (50 µm × 50 µm) region (CV) shown in Fig. 15. This allows to track the evolution of state variables during DDT. The analysis covers the whole set of events from the arrival of the incident shock (IS in Fig. 12) to the emergence of the detonation front.

Figure 15(left) shows that the material first goes through a series of shock compressions (induced by shocks S1–S4) that drastically increases the pressure and the density of the material. IS reflects back and forth between the flame front and the wall, which induces these consecutive shock compressions. Later (at $t \approx 8.011$ ms), as the material detonates, the mixture starts reacting chemically while pressure increases.

The impact of these shock compressions on the mixture ahead of the flame can also be assessed looking at the rate of energy deposition in the control volume (CV) (Fig. 15(right)). The four shock compressions induce a series of rapid sensible energy depositions in the unburnt mixture, prior to DDT. Later, when the material detonates, a fifth peak of sensible energy deposition is observed, along with a rapid chemical energy release. As the flow carries out energy behind the detonation, negative energy rates are observed.

The results of this control volume analysis are in very good agreement with the one performed by Goodwin et. al. [24], who used a single-step mechanism. This shows that DDT triggered by the reflexion back and forth of a shock between a flame front and a wall is not solely observed when detailed chemistry is used.

Figure 15(left) also indicates that the temperature of the unburnt material increases during the shock compressions, to reach temperatures slightly higher than 750 K. This temperature, however, is not sufficient to trigger DDT in the unreacted material. Indeed, 9S18R predicts that $\tau_I \approx 50$ ms at the pressure and temperature conditions ahead of the flame. When the flame exits obstacle 4, it approaches the end wall at 500 m/s and decelerates to 100 m/s prior to the emergence of the detonation (see Fig. 16 (right)). This lower bound for the flame speed (i.e. 100 m/s) allows to evaluate a higher bound for the time needed by the flame to reach the end wall $h/100 \approx 100\,\mu s$, which is two orders of magnitude smaller than τ_I at the fresh gases. This definitely rules out the Zeldovich mechanism ahead of the flame.

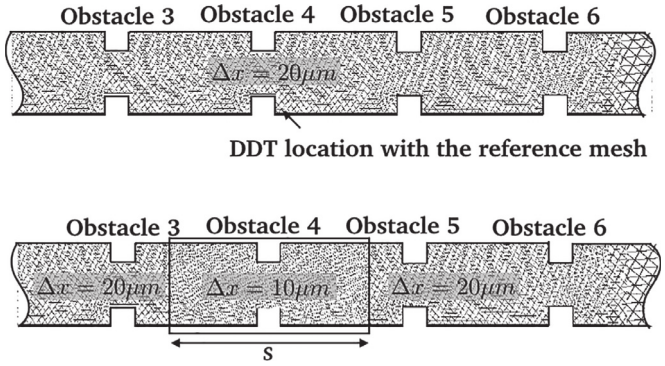

Fig. 17. The meshes used to perform the grid independence study in the multi-step chemistry case. (Top) Reference mesh, used in the core of the manuscript, where the smallest cell size is 20 µm. (Bottom) A new mesh with a higher resolution window, 300 mm large, centered around the DDT location (just after obstacle 4) and where the cell size is 10 µm.

The impact of shock compression is not limited to the unburnt material ahead of the flame but also extends to the flame front itself. This can be assessed using a procedure similar to the one presented in Section 4.3.1. The scenario is investigated through the cut line shown in Fig. 10(Left). Figure 16 shows that the head-on collision of the reflected shocks (*RS*1 and *RS*2) slows down the flame due to a back-flow of fresh gases, the second deceleration being much more pronounced. The flame thus propagates in a continually compressed material with decreasing speed, which triggers an explosion in the only region where the temperature is high enough: the flame preheat zone. A pressure pulse (PP) is

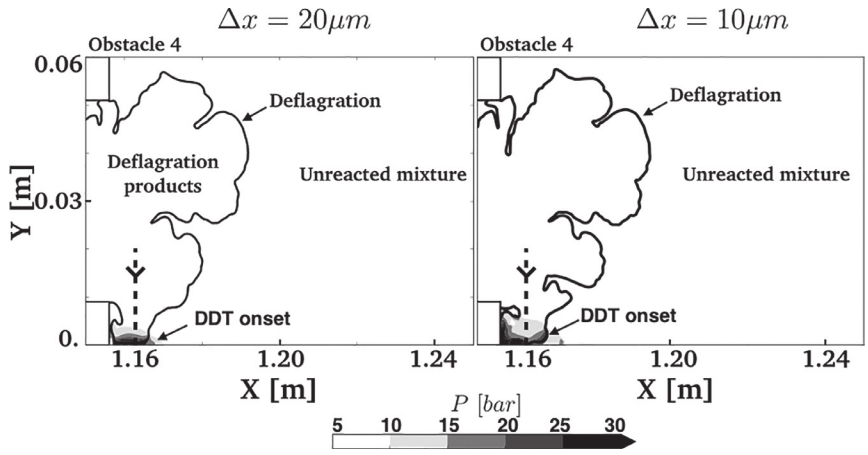

Fig. 18. Zoom on the onset of detonation. Pressure field and isocontour of progress variable $c = 0.5$ are displayed. The dashed lines correspond to a cut through which DDT is analyzed in the core of the manuscript. (Left) Reference mesh. (Right) Refined mesh.

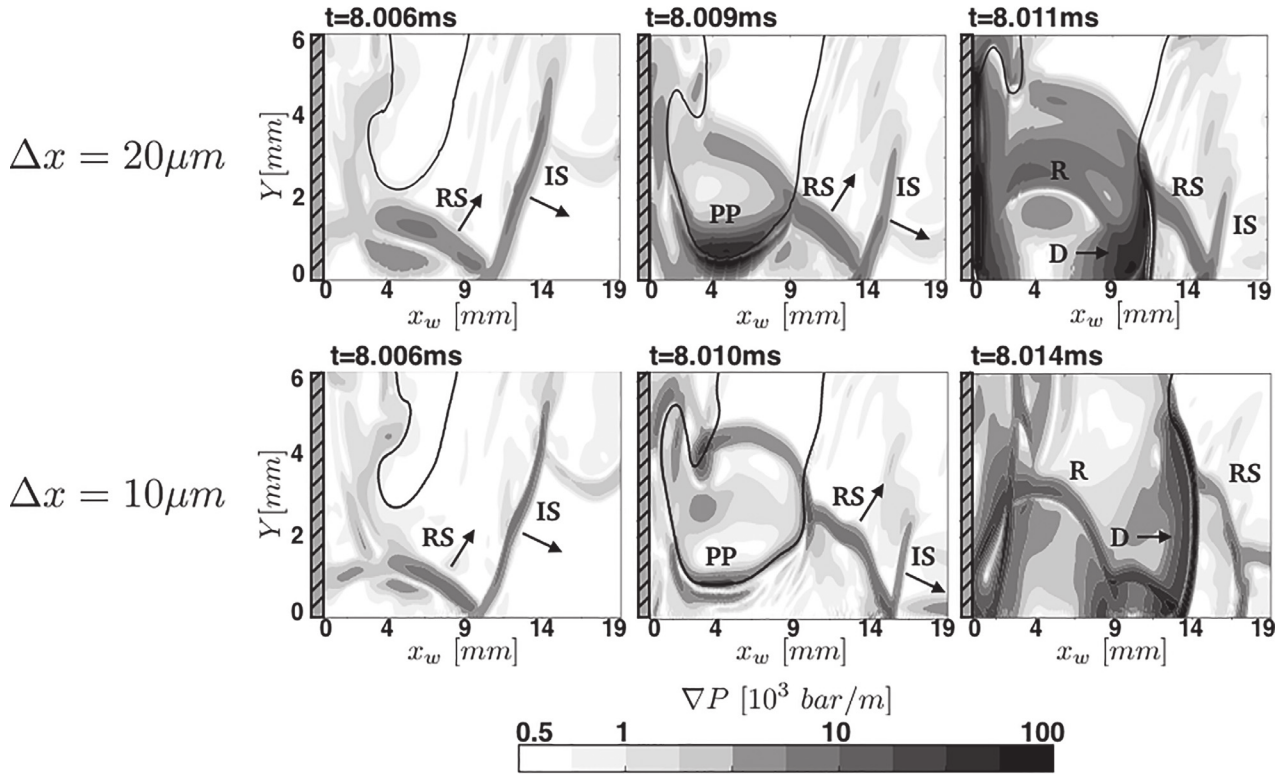

Fig. 19. Key events surrounding the detonation onset for the multi-step simulation using the reference mesh (top) and the refined mesh (bottom). The pressure gradient is displayed. x_w represents the distance from the obstacle 4 right wall (gray dashed area). The deflagration front is represented by the isocontrour of progress variable $c = 0.5$. IS and RS denote the incident shock and the reflected shock, respectively. PP is the pressure pulse observed inside the flame brush prior the detonation onset. D and R indicate the detonation and the retonation waves, respectively.

then observed at $t \approx 8.009$ ms inside the flame preheat zone. PP gains in amplitude as chemical energy is released inside the flame before a detonation emerges from the flame brush.

The DDT mechanism observed in the 9S18R case can finally be summarized as follows: (1) an incident shock gets trapped between the flame front and a wall; (2) this shock reflects back and forth between the reactive wave and the boundary which leads to a series of rapid sensible energy depositions in the unburnt material; (3) the flame thus propagates in a continually compressed mixture and a pressure pulse forms inside the flame preheat zone, where temperatures are high enough to trigger an explosion; (4) a transition to detonation is observed inside the flame brush when the flame reaches the vicinity of the wall through pressure pulse amplification (a form of the SWACER mechanism [16]).

5. Conclusion

The influence of chemistry modeling on the intricate Deflagration to Detonation Transition (DDT) problem is investigated through two chemical mechanisms: (1) a single-step mechanism (3S1R) designed to reproduce the key features of flame and detonation propagation; (2) a multi-step mechanism (9S18R) validated against experimental data in terms of flame speed for a large range of equivalence ratios and in terms of ignition delays for a large range of temperature.

First the idealized hot spot problem with constant temperature gradient is considered. The requirements in terms of temperature and radius for a hot spot to trigger DDT are assessed based on the Bradley et al. [35,45,46] analysis. Results show that the

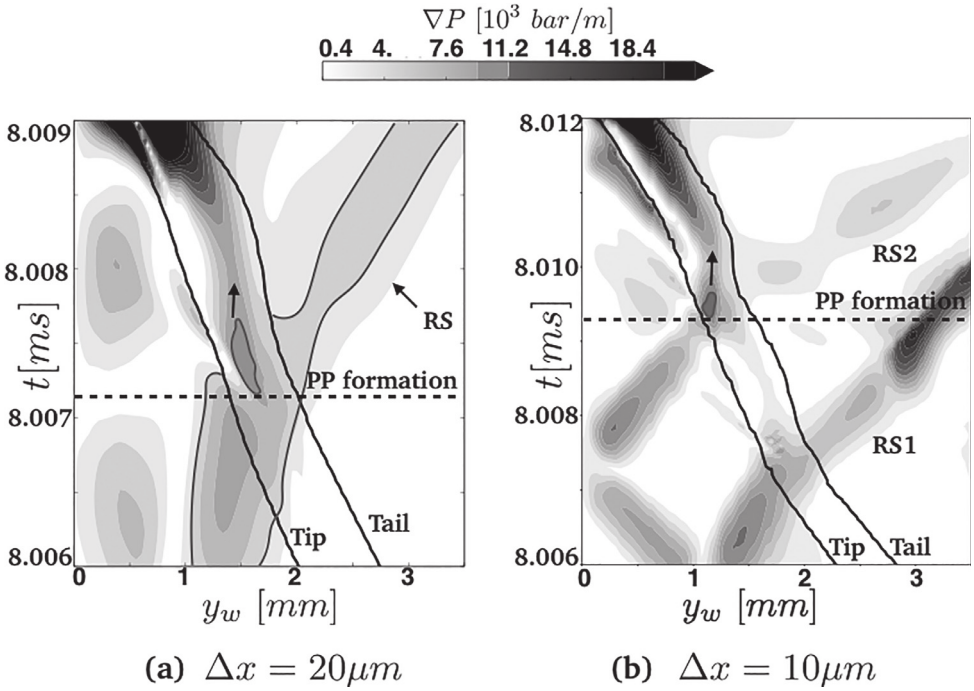

Fig. 20. Time evolution of the pressure gradient in the multi-steps case through the cut line presented in Fig. 10(right). y_w represents the distance to the bottom wall. RS, RS1 and RS2 indicate three reflected shocks and PP denote a pressure pulse. (a) Reference mesh. (b) Refined mesh.

single-step approach can lead to detonation onset from a hot spot for conditions of temperature much lower that the ignition threshold obtained from the experimental data. On the other hand, with 9S18R, the hot spot sizes required for pressure wave amplification by chemical energy input are much higher than those obtained with 3S1R for relatively low pressure conditions, and become comparable at high pressure. This finding suggests that when using a detailed mechanism, the necessary conditions to allow detonation initiation via gradient of reactivity can hardly be met as long as strong shocks are not formed. This is true for hydrogen/air combustion, further studies however are needed to investigate the extent of such a conclusion to other fuels and mixtures. One must keep in mind however that even detailed mechanisms may suffer from large uncertainties at conditions relevant to DDT (i.e. high pressure) due to a lack of calibration data at these conditions. This adds hurdles to an already complex problem.

The DDT problem was also studied through a more realistic configuration: the DDT experiment of the Gravent database [26] where a gas explosion propagates in a confined and obstructed channel filled with a stoichiometric hydrogen/air mixture. Shock reflections were found to be the common ingredient for DDT for all simulations. However, a great influence of the chemistry modeling on the DDT process was observed. In the 3S1R case, the detonation wave emerges from a region of unreacted materiel characterized by a gradient of reactivity, consistently with the Bradley et al. [35,45,46] $\varepsilon - \xi$ analysis. High energy input and resonance between reaction wave and compression wave are required to trigger a detonation. On the other hand, the transition to detonation is found to be triggered inside the flame brush in the 9S18R case. An incident shock, trapped between the flame front and a wall, reflects back and forth between these two interfaces leading to repeated sensible energy depositions. The flame thus propagates in a continually compressed mixture, which leads to the formation of a pressure pulse inside the flame preheat zone, where the temperature is high enough to trigger an explosion. An amplification process is then initiated inside the flame front. DDT is therefore attributed to the resonance between the pressure pulse and the flame brush and to the high chemical energy release inside the flame front. There are reasons to believe that this mechanism might be more frequent when hydrogen/air complex chemistry is considered since the necessary conditions for a hot spot to lead to detonation wave formation may be difficult to meet when using detailed chemistry.

Acknowledgments

The authors would like to thank the reviewers for their constructive remarks and precisions about the complex DDT mechanism. This work is supported by Total company and the assistance of Dr. L. Hoorelbeke, P. Ricoux and A. Dutertre is gratefully acknowledged. The autho rs acknowledge the PRACE systems for the HPC resources awarded during the 14th PRACE call under the allocation project 2016153532.

Annex: Grid independance study for the 9S18R case

To assess the influence of the mesh resolution on the DDT mechanism that appears in the 9S18R case, a grid independence study has been performed using a refined mesh, where the grid resolution has been increased around the location of DDT shown in Fig. 10. The objective here is not to analyse the influence of the mesh resolution on the whole explosion scenario but only on the DDT process. The refined mesh, shown in Fig. 17, is composed of a window, 300 mm large and centred around the DDT location, where the mesh size is 10 μm (i.e. half the mesh size in the reference mesh). This way both the flame and the flow ahead of it benefit from an increased grid resolution.

The DDT location is not impacted by the increase in grid resolution as illustrated in Fig. 18. Figure 19 presents a closer look at the key events surrounding the DDT process for both meshes. It shows that, even though the flow is not exactly the same, the scenarios taking place using both meshes seem to be identical. Note that the pressure pulse is also observed using the refined mesh, hinting that its formation is not due to flame under resolution.

Finally, a similar analysis as the one shown in Fig. 16 is also performed on both meshes and displayed in Fig. 20. It shows that the DDT mechanism in the multi-step case does not seem to be impacted by the increase in the grid resolution. All the ingredients including the reflected shock and the pressure pulse formation are observed in both simulations.

References

[1] E.S. Oran, V.N. Gamezo, Origins of the deflagration-to-detonation transition in gas-phase combustion, Combust. Flame 148 (2007) 4–47.
[2] M. Liberman, M. Ivanov, A. Kiverin, M. Kuznetsov, A. Chukalovsky, T. Rakhimova, Deflagration-to-detonation transition in highly reactive combustible mixtures, Acta Astronaut. 67 (2010) 688–701.
[3] M. Ivanov, A. Kiverin, M. Liberman, Flame acceleration and DDT of hydrogen–oxygen gaseous mixtures in channels with no-slip walls, Int. J. Hydrog. Energy 36 (2011) 7714–7727.
[4] Y. Zel'dovich, V. Librovich, G. Makhviladze, G. Sivashinsky, On the development of detonation in a non-uniformly preheated gas, Acta Astronaut. 15 (1970) 313–321.
[5] G. Ciccarelli, S. Dorofeev, Flame acceleration and transition to detonation in ducts, Prog. Energy Comb. Sci. 34 (2008) 499–550.
[6] D.M. Valiev, V. Bychkov, V. Akkerman, L.-E. Eriksson, Different stages of flame acceleration from slow burning to Chapman–Jouguet deflagration, Phys. Rev. E 80 (2009).
[7] D.M. Valiev, V. Akkerman, M. Kuznetsov, L.-E. Eriksson, C.K. Law, V. Bychkov, Influence of gas compression on flame acceleration in the early stage of burning in tubes, Combust. Flame 160 (2013) 97–111.
[8] O.J. Ugarte, V. Bychkov, J. Sadek, D. Valiev, V. Akkerman, Critical role of blockage ratio for flame acceleration in channels with tightly spaced obstacles, Phys. Fluids 28 (2016) 093602.
[9] A. Oppenheim, Gasdynamic analysis of the development of gaseous detonation and its hydraulic analogy, Symp. (Int.) Combust. 4 (1953) 471–480.
[10] G. Adams, D. Pack, Some observations on the problem of transition between deflagration and detonation, Symp. (Int.) Combust. 7 (1958) 812–819.
[11] Y. Troshin, The generalized Hugoniot adiabatic curve, Symp. (Int.) Combust. 7 (1958) 789–798.
[12] P. Quillatre, O. Vermorel, T. Poinsot, P. Ricoux, Large eddy simulation of vented deflagration, Indus. Eng. Chem. Res. 52 (2013) 11414–11423.
[13] L. Boeck, S. Lapointe, J. Melguizo-Gavilanes, G. Ciccarelli, Flame propagation across an obstacle: OH-PLIF and 2-d simulations with detailed chemistry, Proc. Combust. Inst. 36 (2017) 2799–2806.
[14] O. Vermorel, P. Quillatre, T. Poinsot, LES of explosions in venting chamber: A test case for premixed turbulent combustion models, Combust. Flame 183 (2017) 207–223.
[15] P. Clavin, G. Searby, Combustion waves and fronts in flows, Cambridge University Press, United Kingdom, 2016.
[16] J.H.S. Lee, The detonation phenomenon, Cambridge University Press, New York, NY, 2008.
[17] R. Zipf, V. Gamezo, M. Sapko, W. Marchewka, K. Mohamed, E. Oran, D. Kessler, E. Weiss, J. Addis, F. Karnack, D. Sellers, Methane–air detonation experiments at NIOSH lake Lynn laboratory, J. Loss Prev. Process Indus. 26 (2013) 295–301.
[18] J.H.S. Lee, A.J. Higgins, Comments on criteria for direct initiation of detonation, Phil. Trans. R. Soc. Lond. 357 (1999) 3503–3521.
[19] B. Zhang, H.D. Ng, J.H.S. Lee, Measurement of effective blast energy for direct initiation of spherical gaseous detonations from high-voltage spark discharge, Shock Waves 22 (2012) 1–7.
[20] B. Zhang, H.D. Ng, J.H. Lee, Measurement and relationship between critical tube diameter and critical energy for direct blast initiation of gaseous detonations, J. Loss Prev. Process Indus. 26 (2013) 1293–1299.
[21] P.A. Urtiew, A.K. Oppenheim, Experimental observations of the transition to detonation in an explosive gas, Proc. of the R. Soc. A 295 (1966) 13–28.
[22] J. Lee, R. Knystautas, N. Yoshikawa, Photochemical initiation of gaseous detonations, Acta Astronaut. 5 (1978) 971–982.
[23] T. Zhang, W. Sun, Y. Ju, Multi-scale modeling of detonation formation with concentration and temperature gradients in n-heptane/air mixtures, Proc. Combust. Inst. 36 (2017) 1539–1547.
[24] G. Goodwin, R. Houim, E. Oran, Effect of decreasing blockage ratio on DDT in small channels with obstacles, Combust. Flame 173 (2016) 16–26.
[25] M. Kuznetsov, M. Liberman, I. Matsukov, Experimental study of the preheat zone formation and deflagration to detonation transition, Combust. Sci. Technol. 182 (2010) 1628–1644.
[26] K.G. Vollmer, F. Ettner, T. Sattelmayer, Deflagration-to-detonation transition in hydrogen/air mixtures with a concentration gradient, Combust. Sci. Technol. 184 (2012) 1903–1915.
[27] M. Liberman, A. Kiverin, M. Ivanov, On detonation initiation by a temperature gradient for a detailed chemical reaction models, Phys. Lett. A 375 (2011) 1803–1808.
[28] M.A. Liberman, A.D. Kiverin, M.F. Ivanov, Regimes of chemical reaction waves initiated by nonuniform initial conditions for detailed chemical reaction models, Phys. Rev. E 85 (2012) 056312.
[29] L. Gicquel, G. Staffelbach, T. Poinsot, Large eddy simulations of gaseous flames in gas turbine combustion chambers, Prog. Energy Comb. Sci. 38 (2012) 782–817.
[30] O. Colin, M. Rudgyard, Development of high-order Taylor–Galerkin schemes for unsteady calculations, J. Comput. Phys. 162 (2000) 338–371.
[31] P. Boivin, C. Jiménez, A. Sánchez, F. Williams, An explicit reduced mechanism for H_2-air combustion, Proc. Combust. Inst. 33 (2011) 517–523.
[32] D. Kessler, V. Gamezo, E. Oran, Simulations of flame acceleration and deflagration-to-detonation transitions in methane–air systems, Combust. Flame 157 (2010) 2063–2077.
[33] C. Wang, J. Wen, S. Lu, J. Guo, Single-step chemistry model and transport coefficient model for hydrogen combustion, Sci. Chin. Technol. Sci. 55 (2012) 2163–2168.
[34] E.S. Oran, Understanding explosions from catastrophic accidents to creation of the universe, Proc. Combust. Inst. 35 (2015) 1–35.
[35] D. Bradley, G. Kalghatgi, Influence of autoignition delay time characteristics of different fuels on pressure waves and knock in reciprocating engines, Combust. Flame 156 (2009) 2307–2318.
[36] G. Joulin, T. Mitani, Linear stability analysis of two-reactant flames, Combust. Flame 40 (1981) 235–246.
[37] C. Sun, C. Sung, L. He, C. Law, Dynamics of weakly stretched flames: quantitative description and extraction of global flame parameters, Combust. Flame 118 (1999) 108–128.
[38] M. Berman, Sandia Laboratories Report SAND84-0689, Technical Report, Sandia National Laboratories, Albuquerque, New Mexico (1984).
[39] D.R. Dowdy, D.B. Smith, S.C. Taylor, A. Williams, The use of expanding spherical flames to determine burning velocities and stretch effects in hydrogen/air mixtures, Symp. (Int.) Combust. 23 (1991) 325–332.
[40] F. Egolfopoulos, C. Law, An experimental and computational study of the burning rates of ultra-lean to moderately-rich $H_2/O_2/N_2$ laminar flames with pressure variations, Symp. (Int.) Combust. 23 (1991) 333–340.
[41] T. Iijima, T. Takeno, Effects of temperature and pressure on burning velocity, Combust. Flame 65 (1986) 35–43.
[42] F. Takahashi, M. Mizomoto, S. Ikai, Alternative energy sources III, in: Nuclear Energy/Synthetic Fuels, T. Nejat Veziroglu, 5 (1983) 447–457.
[43] M. Slack, A. Grillo, Investigation of hydrogen-air ignition sensitized by nitric oxide and by nitrogen dioxide, Technical Report RE-537, Grumman Research Department, 1977.
[44] A.D. Snyder, J. Robertson, D.L. Zanders, G.B. Skinner, Shock tube studies of fuel-air ignition characteristics, Technical Report, Air Force Aero Propulsion Laboratory (AFAPL) Research and Technology Division, 1965.
[45] L. Bates, D. Bradley, G. Paczko, N. Peters, Engine hot spots: Modes of auto-ignition and reaction propagation, Combust. Flame 166 (2016) 80–85.
[46] L. Bates, D. Bradley, Deflagrative, auto-ignitive, and detonative propagation regimes in engines, Combust. Flame 175 (2017) 118–122.